THE JOURNAL OF BIOLOGICAL CHEMISTRY
Vol. 277, No. 40, Issue of October 4, pp. 37702–37710, 2002

Printed in U.S.A.

Dynamics of Glucose-induced Membrane Recruitment of Protein Kinase C βII in Living Pancreatic Islet β-Cells*[S]

Received for publication, May 7, 2002, and in revised form, July 10, 2002
Published, JBC Papers in Press, July 30, 2002, DOI 10.1074/jbc.M204478200

Paolo Pinton‡§¶‖, Takashi Tsuboi‡‖, Edward K. Ainscow‡, Tullio Pozzan§, Rosario Rizzuto¶, and Guy A. Rutter‡ ‡‡**

From the ‡Henry Wellcome Signalling Laboratories and the Department of Biochemistry, University of Bristol, Bristol BS8 1TD, United Kingdom, the §Department of Biomedical Sciences and CNR Centre for Study of Biological Membranes, University of Padova, Viale G. Colombo 3, 35121 Padova, Italy, and the ¶Department of Experimental and Diagnostic Medicine Section of the General Pathology and Interdisciplinary Center for the Study of Inflammation (ICSI), University of Ferrara, Via Borsari, 46 44100 Ferrara, Italy

The mechanisms by which glucose may affect protein kinase C (PKC) activity in the pancreatic islet β-cell are presently unclear. By developing adenovirally expressed chimeras encoding fusion proteins between green fluorescent protein and conventional (βII), novel (δ), or atypical (ζ) PKCs, we show that glucose selectively alters the subcellular localization of these enzymes dynamically in primary islet and MIN6 β-cells. Examined by laser scanning confocal or total internal reflection fluorescence microscopy, elevated glucose concentrations induced oscillatory translocations of PKCβII to spatially confined regions of the plasma membrane. Suggesting that increases in free cytosolic Ca^{2+} concentrations ($[Ca^{2+}]_c$) were primarily responsible, prevention of $[Ca^{2+}]_c$ increases with EGTA or diazoxide completely eliminated membrane recruitment, whereas elevation of cytosolic $[Ca^{2+}]_c$ with KCl or tolbutamide was highly effective in redistributing PKCβII both to the plasma membrane and to the surface of dense core secretory vesicles. By contrast, the distribution of PKCδ-EGFP, which binds diacylglycerol but not Ca^{2+}, was unaffected by glucose. Measurement of $[Ca^{2+}]_c$ immediately beneath the plasma membrane with a ratiometric "pericam," fused to synaptic vesicle-associated protein-25, revealed that depolarization induced significantly larger increases in $[Ca^{2+}]_c$ in this domain. These data demonstrate that nutrient stimulation of β-cells causes spatially and temporally complex changes in the subcellular localization of PKCβII, possibly resulting from the generation of Ca^{2+} microdomains. Localized changes in PKCβII activity may thus have a role in the spatial control of insulin exocytosis.

Ca^{2+} and phospholipid-dependent protein kinases (PKC)[1] are important mediators of intracellular signals (1). PKC isoforms can be divided into three subfamilies. Conventional PKCs are activated via recruitment to membranes, mediated by the Ca^{2+}-dependent binding of a C2 domain to phospholipids, and this effect is further potentiated by the binding of diacylglycerol (DAG) to C1 domains (1). By contrast, novel PKCs bind DAG, but not Ca^{2+} and phospholipids, while atypical PKCs are not affected by any of the above activators (1).

Biochemical studies of the activation of PKC are complicated by the need for cell disruption and isolation of membrane and cytosol fractions (2) or for cell fixation and immunocytochemistry (2–4). Each of these approaches is limited by the difficulty of detecting any changes in subcellular localization, which are spatially or temporally complex. To overcome this limitation, fusion constructs between enhanced green fluorescent protein (EGFP) (5) and PKCγ (6), PKCα (7), PKCδ (8), and PKCβII (9) have recently been used to monitor the dynamics of membrane translocation of PKCs in a number of non-excitable cell types and appear faithfully to reflect the behavior of the endogenous PKC isoforms. However, while PKC may play an important role in agonist stimulation of exocytosis from neurosecretory cells (10), no data are presently available on the dynamics of conventional PKCs in any excitable cell type.

Elevated glucose concentrations stimulate insulin secretion from β-cells via metabolism of the sugar (11, 12) and increases in cytosolic free ATP concentration (13). Closure of ATP-sensitive K^+ channels (14) then leads to depolarization of the plasma membrane, influx of Ca^{2+} through voltage-gated Ca^{2+} channels (15), and secretory vesicle fusion (16). PKC activity is present in both primary pancreatic islets (17) and derived β-cell lines (18, 19). Furthermore, conventional (α, βI, βII; sensitive to Ca^{2+} and DAG), novel (δ; sensitive to DAG but not Ca^{2+}), and atypical (ζ, λ; insensitive to Ca^{2+} and DAG) PKC isoforms (20–23) have all been reported in islet cells. However, the role of PKC in the stimulation of insulin secretion is controversial. Acute activation of conventional and novel PKCs with the phorbol ester 12-*O*-tetradecanoyl-phorbol-13-acetate strongly stimulates insulin secretion (19, 24) without affecting β-cell electrical activity or cytosolic free Ca^{2+} ($[Ca^{2+}]_c$) (25, 26). On the other hand, inhibition of PKC activity with the broad specificity inhibitor staurosporine (27), or an inhibitor specific for classical PKC isoforms (Go6976), slightly *enhances* the first phase of glucose-stimulated insulin release from rat islets (28)

* This work was supported by grants from the Human Frontiers Sciences Program, the Medical Research Council (UK), The Wellcome Trust, the Biotechnology and Biological Research Council, Diabetes UK, the European Union, the Italian "Telethon" (Project No. 1250), the Italian University and Health Ministries, the Italian Space Agency, The Italian National Research Council, The Armenise Harvard Foundation, and the Italian Association for Cancer Research. The costs of publication of this article were defrayed in part by the payment of page charges. This article must therefore be hereby marked "*advertisement*" in accordance with 18 U.S.C. Section 1734 solely to indicate this fact.

[S] The on-line version of this article (available at *http://www.jbc.org*) contains movies for Figs. 2–5.

‖ Both authors contributed equally to this work.
** Recipient of an EMBO short-term fellowship.
‡‡ To whom correspondence should be addressed. Tel.: 44-117-954-6491; Fax: 44-117-928-8274; E-mail: g.a.rutter@bris.ac.uk.

[1] The abbreviations used are: PKC, protein kinase C; DAG, diacylglycerol; EGFP, enhanced green fluorescent protein; ECFP, enhanced cyan fluorescent proteins; TIRF, total internal reflection fluorescence; KRB, Krebs-Ringer bicarbonate buffer; PMA, phorbol 12-myristate 13-acetate; $[Ca^{2+}]_c$, cytosolic free Ca^{2+} ion concentration; $[Ca^{2+}]_{PM}$, plasma membrane-domain free Ca^{2+} ion concentration.

while diminishing the sustained phase. Down-regulation of conventional PKC isoforms with phorbol esters has little effect on glucose-stimulated insulin release (29).

To determine whether active PKCs may play a role in the spatial coordination of exocytosis in individual β-cells without necessarily affecting total insulin release, we have therefore generated fusion constructs between EGFP and PKCβII, PKCδ, and PKCζ. PKCβII and PKCα represent the major conventional PKC isoforms in β-cells (20), and PKCβII activity has recently been shown to be important for the regulation of the preproinsulin gene (23). Expression of these constructs has allowed the dynamics of each isoform to be studied in real time in both primary islet and clonal β-cells. Using confocal and total internal reflection fluorescence (TIRF)/evanescent wave (30–34) imaging, we show that elevated glucose concentrations cause complex, oscillatory translocations to the plasma and other membranes of PKCβII in primary β-cells and clonal MIN6 cells. These changes appear to be produced largely by transient depolarizations of the plasma membrane and stimulated Ca^{2+} influx. The formation of microdomains of $[Ca^{2+}]_c$ immediately beneath the plasma membrane, demonstrated directly by targeting a green fluorescent protein-based Ca^{2+} probe ("pericam") (35) exclusively to this domain, may be critical for the generation of complex movements of PKC.

EXPERIMENTAL PROCEDURES

Materials and Methods

Cell culture reagents were obtained from Invitrogen or Sigma, and molecular biologicals from Roche Molecular Biochemicals.

Adenoviral Generation—Adenoviruses were constructed and amplified using the pAdEasy system (36) as previously described (37). The PKCβII·EGFP, PKCδ·EGFP, and PKCζ·EGF (8) cDNAs were transferred into plasmid pShuttleCMV as *Kpn*I/*Xho*I fragments. Adenoviral generation from the recombinant shuttle vectors was performed, and infection of cells and islets was performed as previously described (37).

Recombination with pAdEasy-1, transfection into HEK 293 cells, and viral amplification of the pShuttle-CMV based plasmids encoding each recombinant PKC isoform-GFP fusion proteins was performed essentially as previously described (37). Determination of viral concentration was by comparison of the absorbance at 260 nm with a viral stock of known titer (37). MIN6 cells were infected with a multiplicity of infection of 30, ~16 h prior to imaging.

Cell Culture and Adenoviral Infection—Primary isolated islet β-cells and MIN6 cells (passages nos. 20 to 30) were cultured and infected with adenoviruses as previously described (38). In each case, the concentration of glucose was lowered to 3 mM for 16 h before experiments.

Confocal Imaging Analysis—Coverslips (24 mm in diameter) were placed in a thermostatted Leyden chamber, (model TC-202A, Medical Systems Corp.) on the stage of an inverted Leica SP2 confocal imaging system using a 63X (numerical aperture = 1.45) oil immersion objective. All experiments were carried out in Krebs-Ringer bicarbonate buffer (KRB): 125 mM NaCl, 3.5 mM KCl, 1.5 mM $CaCl_2$, 0.5 mM NaH_2PO_4, 0.5 mM $MgSO_4$, 3 mM glucose, 10 mM Hepes, 2 mM $NaHCO_3$, pH 7.4, containing, initially, 3 mM glucose and equilibrated with O_2/CO_2 (19:1). Images were acquired at a rate of 0.5 s^{-1} and processed off line. Green and cyan fluorescent protein (ECFP) fluorescence were imaged simultaneously through alternate excitation (0.2 s^{-1}) at 430 and 488 nm with emitted fluorescence filtered between 450 and 490 nm and between 520 and 560 nm, respectively. Under these conditions, cross-contamination of the two signals was negligible.

Calcium Crimson Imaging—MIN6 cells were infected with adenoviral PKCβII·EGFP as described above and cultured overnight in medium containing 3 mM glucose. 1 h prior to imaging, cells were micro-injected using an Eppendorf 5171/5242 micromanipulator/pressure microinjector with a solution of 0.5 μM Calcium Crimson conjugated to 10,000 Da dextran (Molecular Probes, Eugene, OR), to give an approximate final concentration of 20 nM in the cytosol. The cells were washed once and incubated at 37 °C until use.

During imaging, cells were incubated in KRB medium and maintained at 37 °C on a heated stage. Cells that had been successfully injected with Calcium Crimson dye and were expressing the PKCβII·EGFP were identified by epifluorescence and imaged on a Leica confocal imaging spectrophotometer system (TCS-SP) running on a DM/IRBE inverted microscope (×40 objective). Fluorescence of Calcium Crimson (568-nm excitation, Kr laser; 580–640-nm emission) and EGFP (488-nm excitation, Ar laser; 520–560-nm emission) were monitored simultaneously and analyzed using Leica TCS software. Additions were made via a small volume of a stock solution (3.5 M KCl) followed by rapid mixing with a pipette.

Changes in Calcium Crimson fluorescence were determined throughout the whole cell and presented as an increase relative to basal fluorescence. EGFP fluorescence was determined in the vicinity (~1 μm) of the plasma membrane and in the bulk cytosol. The ratio of the average fluorescence of these regions was used as a measure of PKCβII·EGFP translocation. Relative changes in this ratio, normalized to basal conditions, are given.

Construction of SNAP25 Pericam, phogrin·ECFP, and Cell Transfection—To generate a plasmid encoding plasma membrane-targeted ratiometric pericam (ratiometric-pericam-pm), cDNA encoding ratiometric pericam (35) was digested using *Bam*HI/*Eco*RI. The restricted fragment encoding the pericams was subcloned into pcDNA 3.1(+) (Invitrogen). The *Nhe*I/*Bam*HI fragment of synaptosomal-associated protein of 25-kDa cDNA was inserted with the correct orientation into ratiometric-pericam/pcDNA3.1(+) vector. cDNA encoding an in-frame fusion construct between phogrin (39) and ECFP was generated by replacement of the *Asn*1/*Pst*I fragment of phogrin·EGFP (40) with the *Asn*1/*Nsi*1 fragment from phogrin·Ycam2 (41) encoding ECFP. Correct orientation and sequence of inserts was confirmed by automated DNA sequencing. Transfection of MIN6 cells was performed using LipofectAMINE 2000 (Invitrogen) as per the manufacturer's instructions 2–3 days prior to experiments.

Determination of $[Ca^{2+}]$ Changes with the Ratiometric Pericams—MIN6 cells in KRB buffer were imaged at 37 °C using an Olympus IX-70 with an IMAGO charge-coupled device camera (Till Photonics GmbH, Grafelfing, Germany) controlled by TillvislON software (Till Photonics). Cells were illuminated alternatively for 100 and 90 ms at 410 and 480 nm, and the emitted light was filtered at 535 nm. The ratio images were used to calculate $[Ca^{2+}]$ off line according to established methods (42).

TIRF Microscopy—To assess translocation of PKCβII·EGFP, we employed a TIRF (also known as evanescent wave microscopy) microscope similar to that described previously by Tsuboi *et al.* (32–34). The incident light for total internal reflection illumination was introduced from the objective lens (Olympus, numerical aperture = 1.65, 100X magnification) through a single mode optical fiber and two illumination lenses. To observe the EGFP fluorescence image, we used a 488-nm laser (argon ion laser, 30 mW, Spectra-Physics) for total internal fluorescence illumination and a long pass filter (515 nm) for barrier. The laser beam was passed through an electromagnetically driven shutter (Till Photonics). The shutter was opened synchronously with camera exposure under control by TillvisilON software (Till Photonics). Images were acquired every 2 s. To analyze the data, translocation events were manually selected and the average fluorescence intensity of individual plasma membrane regions was calculated.

Statistical Analysis

Data are given as means ± S.E. of at least three individual experiments. Comparisons between means were performed using one-tailed Student's *t* test for paired data with Microsoft Excel™ or Origin 7™ (OriginLab, Northampton, MA) software.

RESULTS

Responses of PKCβII to Glucose and Other Agonists in Primary β-Cells—Fig. 1*A* shows the responses to a stepped increase in glucose concentration from 3 to 25 mM of adenovirally expressed PKCβII·EGFP, imaged by laser-scanning confocal microscopy in primary β-cells. An increase in fluorescence ratio (plasma membrane: cytosol) was observed in 7 of 16 cells examined (from two separate preparations; mean increase 13.5 ± 4.2%), with partial oscillations (*i.e.* retranslocation to the cytosol) observed in three of seven cells. In some cases, recruitment was "patchy" with evidence of localization on membrane-associated organelles (Fig. 1*A*, *arrow*). Implicating $[Ca^{2+}]_c$ increases in these effects of glucose, cell depolarization with 35 mM KCl (Fig. 1*B*) or stimulation of muscarinic receptors with carbachol, 100 μM (Fig. 1*C*), also caused a clear increase in the proportion of plasma membrane-bound PKCβII and in each case the appearance of focal points of high fluorescence (*arrows*).

In contrast to PKCβII·EGFP, neither PKCδ·EGFP nor

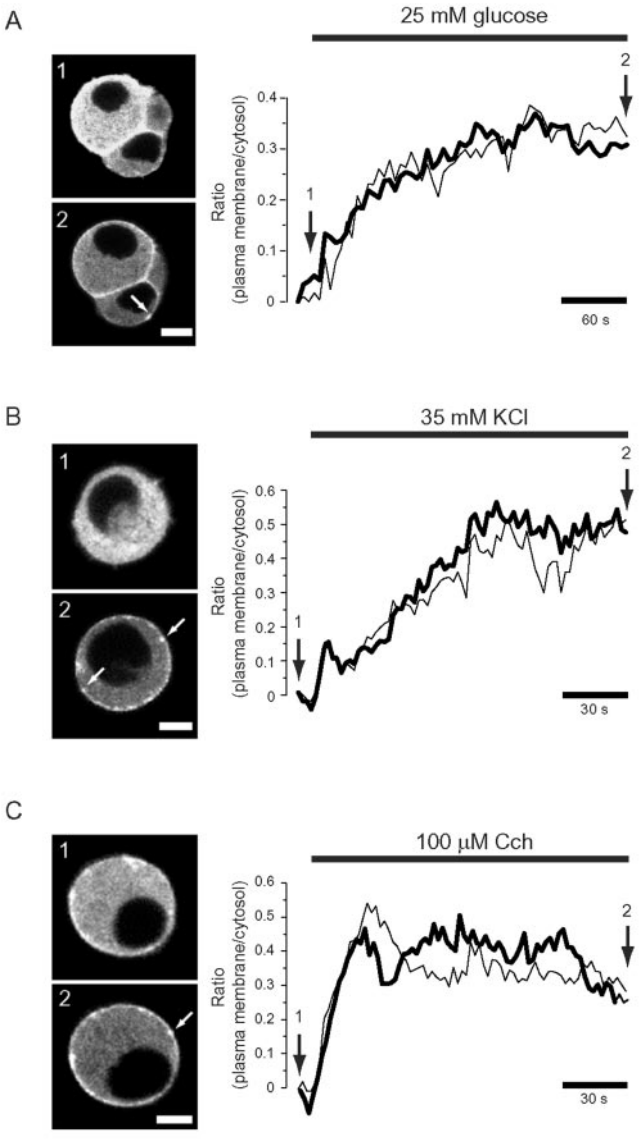

FIG. 1. **Glucose-induced translocation of PKCβII and EGFP in primary isolated islet β-cells.** *A*, changes in the PKCβII·EGFP distribution were monitored by laser-scanning confocal microscopy in response to an increase in glucose concentration from 3 to 25 mM. The images shown were recorded before and after glucose stimulation as indicated by the *vertical arrows*. The graph indicates the time course of plasma membrane translocation of PKCβII·EGFP expressed as the increase in fluorescence ratio with respect to time zero (calculated as a ratio of plasma membrane:average intracellular fluorescence obtained from regions of interest with 1 μm, and >2 μm, respectively, from the cell surface). Primary β-cells were stimulated at 3 mM glucose with 35 mM KCl (*B*), or 100 μM carbachol (*Cch*) (*C*). Traces correspond to the cells shown in the images (*black lines*) or are the means of five single cells (*light gray traces*). *Scale bar*, 5 μm.

PKCζ·EGFP displayed any detectable change in subcellular distribution in primary β-cells in response to the above stimuli, while phorbol 12-myristate 13-acetate (PMA) caused translocation of PKCδ from the cytosol to the nuclear periphery (not shown; see also Fig. 7 for response in MIN6 cells).

Responses of PKCβII·EGFP Distribution to Elevated [Glucose] and Other Stimuli in MIN6 β-Cells—To explore the mechanisms involved in the glucose-stimulated translocation of PKCβII·EGFP in more detail we next used clonal MIN6 β-cells. In contrast to primary β-cells, these well differentiated and glucose-responsive cells (43) can be easily microinjected with both plasmid cDNAs and with Ca^{2+} indicator dyes (37) without marked deterioration of cell function.

Examined first by laser-scanning confocal microscopy, PKCβII·EGFP translocated to the plasma membrane in response to 25 mM glucose in 7 of 22 MIN6 cells examined (Fig. 2*A*). Retranslocation to the cytosol was clearly evident in almost half (three of seven) of the cells examined. To provide greater temporal and spatial resolution we next employed TIRF microscopy (31–34). This technique involves the generation of a thin (<100 nm) field of fluorescence at the surface of the coverslip and thus at the surface of an attached cell. Hence a fluorophore such as PKCβII·EGFP will only fluoresce as it approaches very close to (within ~50 nm) the plasma membrane while molecules in the cytosol remain in darkness. Since MIN6 cells display a flattened morphology, this technique was anticipated to permit a more precise quantification of plasma membrane-associated PKCβII.

PKCβII EGFP was translocated to the plasma membrane with a half-time of ~60 s and a peak increase in membrane:cytosolic PKCβII·EGFP of ~1.5 (Fig. 2*B*). Translocation was not provoked by a non-metabolizable sugar (galactose, not shown) and was completely suppressed by chelation of extracellular Ca^{2+} with EGTA or by cell hyperpolarization with the ATP-sensitive K^+ channel opener, diazoxide (Fig. 2*B*, *trace 4*). In some cells, "hot spots" and waves of PKC were clearly detectable (see movie "Fig. 2*B*" at *http://www.jbc.org*). These effects were not observed in cells expressing a membrane-targeted GFP chimera (not shown) and are thus unlikely to result simply from changes in the shape of the cell. Moreover, the effects of glucose upon translocation were only marginally reduced by inhibition of phospholipase C activity with U73122 (Fig. 2*B*, *trace 5*) (44) at a concentration (10 μM) that completely inhibited the effects of carbachol on PKCβII translocation (see Fig. 5*B*, *trace 3*; see movie "Fig. 5*B*" at *http://www.jbc.org* for the effect of carbachol alone) or $[Ca^{2+}]_c$ (not shown).

Measurement of Global or Localized Ca^{2+} Changes with Recombinant Targeted Pericams—Changes in free Ca^{2+} concentration were measured throughout the cell cytosol after expression of a ratiometric pericam (35) in this compartment. Elevating the glucose concentration from 3 to 30 mM caused a gradual increase in $[Ca^{2+}]_c$ from ~200 nM to close to 1 μM (resting 0.18 ± 0.1 μM, maximum 1.03 ± 0.34 μM, n = 10 cells in each case; Fig. 2*C*), with a half-time similar to that for the increases in PKCβII associated with the plasma membrane (Fig. 2, *A* and *B*). In some cells (4 of 10 examined) the glucose-induced increases were more oscillatory, consisting of spikes on a steadily increasing baseline (Fig. 2*D*).

We next tested the possibility that highly localized changes in $[Ca^{2+}]_c$ immediately beneath the plasma membrane may be involved in PKCβII membrane recruitment. The formation of such a Ca^{2+} microdomain would be expected to permit phospholipid-dependent interaction of the PKCβII C2 domain with the membrane inner leaflet (45), independently of the DAG binding domain (C1) (46).

To achieve measurements of $[Ca^{2+}]_c$ close to the inner surface of plasma membrane (<10 nm), we targeted the Ca^{2+} sensor, ratiometric pericam (35) to this region of the cell. cDNA encoding the pericam was fused in frame with that encoding the soluble *N*-ethyl maleimide-sensitive factor receptor (t-SNARE), synaptosome-associated protein of 25 kDa (SNAP25), which binds to membranes after palmitoylation (47). The SNAP25·pericam chimera displayed a largely plasma membrane localization with some fluorescence on intracellular structures, possibly corresponding to the Golgi apparatus or mature secretory vesicles (Fig. 2*E*, *monochrome panel*) (13). Importantly, the molecular targeting of this construct eliminated the need for spatially selective excitation (*i.e.* by confocal or TIRF microscopy), permitting ratiometric measurement of

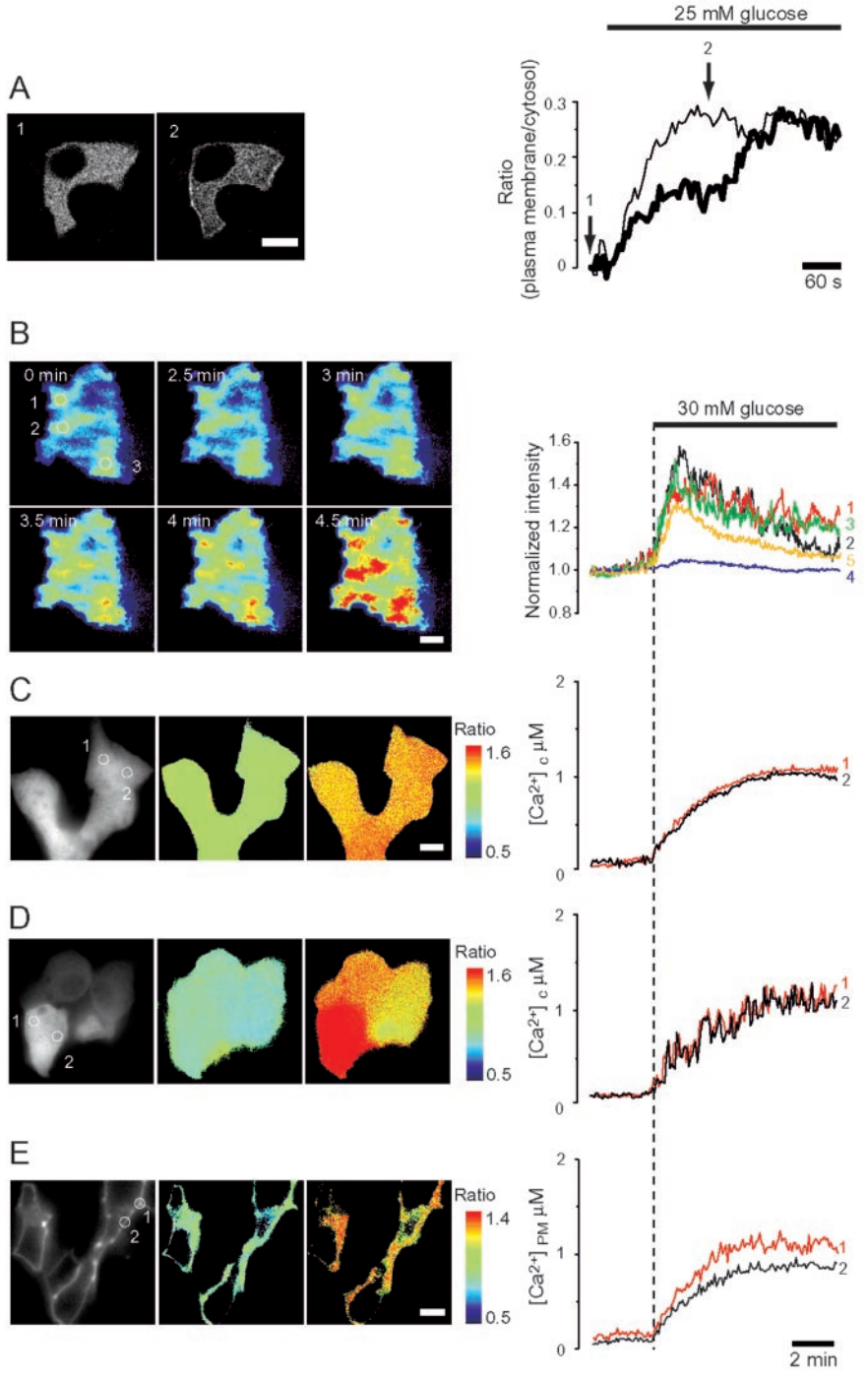

FIG. 2. **Effect of glucose on PKCβII·EGFP distribution and localized Ca^{2+} concentration changes in MIN6 β-cells.** MIN6 cells were infected with either PKCβII·EGFP-encoding adenovirus (*A*, *B*) transfected with untargeted (*C*, *D*) or plasma membrane-targeted (E) pericams prior to imaging. Cells were maintained initially in KRB containing 3 mM glucose and imaged (*A*) on the confocal microscope or (*B*) by total internal reflection fluorescence microscopy during the increases in glucose concentration indicated. In *A*, the traces show the increases in total plasma membrane fluorescence in the single cell shown relative to cytosolic fluorescence (see Fig. 1). The increase in plasma membrane-associated fluorescence (calculated as a ratio of average intracellular fluorescence by quantification of regions of interest with 1 μm, >2 μm, respectively, from the cell surface) or the increase in fluorescence normalized to the prestimulatory level in *B*. In each case, traces represent the mean of more than four cells or are from a single typical cell. Cells in *C*, *D*, and *E* were transfected with constructs encoding untargeted or plasma-membrane-targeted pericams, respectively, before ratio metric imaging (pseudocolor) of $[Ca^{2+}]$ changes by epifluorescence microscopy as described under "Experimental Procedures." Note the greater heterogeneity in $[Ca^{2+}]$ (*trace 1 versus 2*) and appearance of small transients at the plasma membrane (*E*). Monochrome images show fluorescence excited at 410 nm; an essentially identical distribution of fluorescence was apparent under excitation at 480 nm and reflects the intracellular distribution of the probe. *Scale bars*, 5 μm.

fluorescence by conventional epifluorescence microscopy. The membrane-targeted pericam displayed a dissociation constant for Ca^{2+} close to that previously reported for the untargeted construct (1.7 μM) (35) in digitonin-permeabilized cells (not shown). Resting Ca^{2+} concentrations reported with this pericam were not significantly different (0.21 μM) compared with the untargeted reporter (0.18 μM, Fig. 2, *C* and *D*). However, greater heterogeneity was apparent in the $[Ca^{2+}]_c$ increases elicited by elevated glucose concentrations (Fig. 2*E*, *trace 1 versus 2*) in cells expressing the plasma membrane-targeted pericam, with an average difference in the peak $[Ca^{2+}]_c$ achieved at two randomly selected locations on the plasma membrane of 0.22 ± 0.06 μM ($n = 8$ separate cells). By contrast, no significant differences in peak $[Ca^{2+}]_c$ in different areas of the cell cytoplasm were detected using the untargeted pericam, either in cells displaying a monotonic response to the sugar (Fig. 2*C*) or in those in which $[Ca^{2+}]_c$ oscillations were apparent (Fig. 2*D*).

Effect of Stimulated Ca^{2+} Influx on PKCβII Localization—Stimulation of Ca^{2+} influx with either depolarizing concentrations of KCl (in 29 of 34 cells examined, Fig. 3, *A* and *B*; see movie "Fig. 3*B*" at *http://www.jbc.org*) or tolbutamide, which closes ATP-sensitive K^+ channels (in 16 of 19 cells examined, Fig. 4, *A* and *B*) caused clear and rapid translocation of PKCβII to the cell surface. Tolbutamide stimulation was usually also followed by a series of oscillations in both PKCβII translocation (Fig. 4*B*; see movie "Fig. 4*B*" at *http://www.jbc.org*) to the plasma membrane, as well as cytosolic (Fig. 4*C*) and plasma membrane $[Ca^{2+}]$ (Fig. 4*D*). Arguing against the possibility that the transient nature of the KCl-induced PKCβII translo-

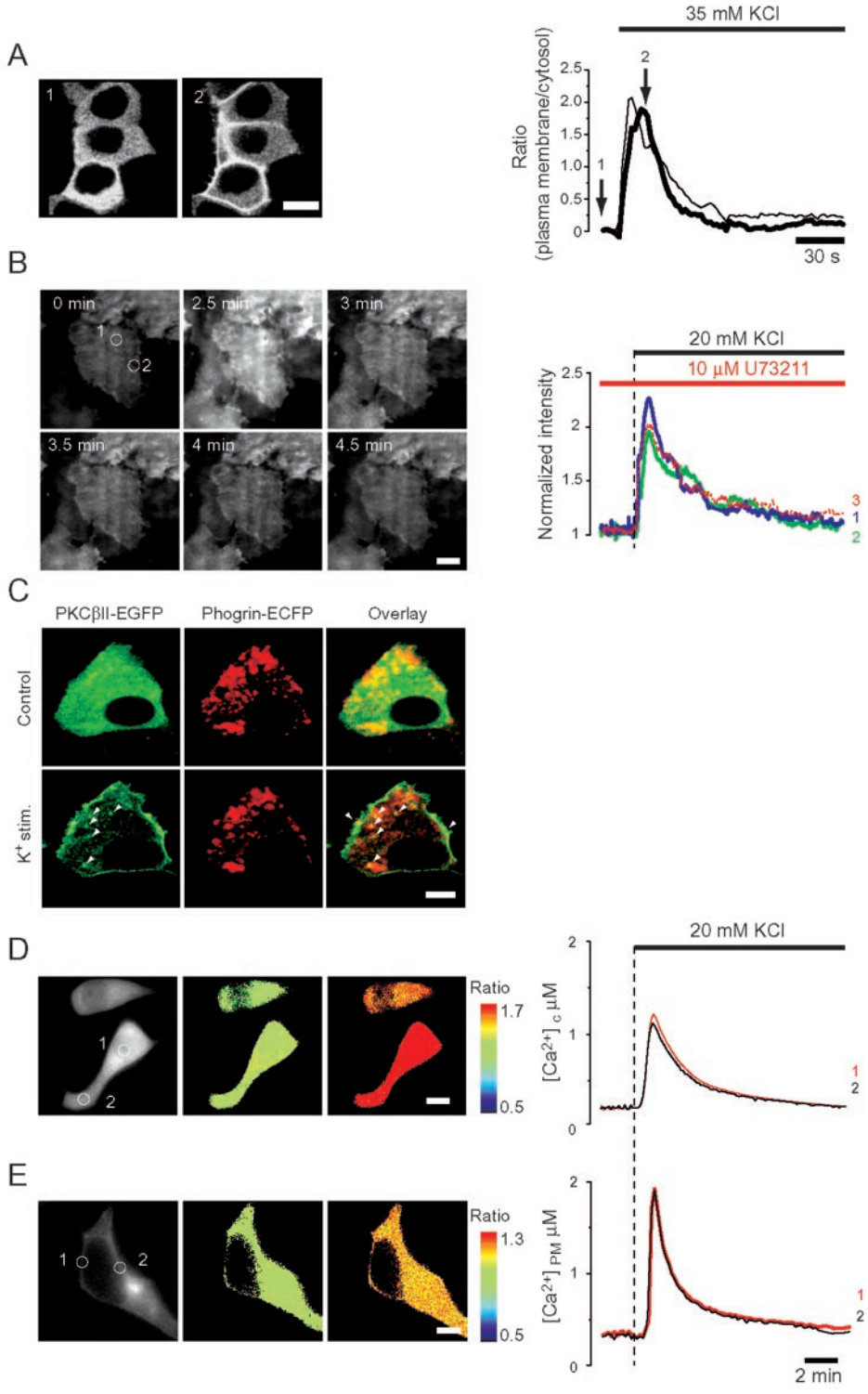

FIG. 3. **Effect of membrane depolarization with KCl on PKC·βII distribution (*A*, *B*, *C*) and intracellular Ca^{2+} changes (*D*, *E*).** Cells expressing either PKCβII (*A*, *B*, *C*), plus phogrin·ECFP (*C*) or targeted pericams (*D*, *E*), were incubated with the indicated concentrations of KCl. In *C*, images were captured by alternate illumination at 430 and 488 nm as described under "Experimental Procedures"; points of colocalization between PKCβII and phogrin·ECFP-containing dense core vesicles are indicated with *arrows*. Other details were as Fig. 2. Note the substantially larger increase in $[Ca^{2+}]_{PM}$ (*D*) than $[Ca^{2+}]_c$ (*C*) following KCl addition.

cation was due to a short-lived increase in DAG generation by phospholipid hydrolysis, glucose-stimulated translocation of PKCβII·EGFP was entirely unaffected by the pharmacological PLC inhibitor, U73122 (Fig. 3*B*, *trace 3*).

Imaged by confocal microscopy (Fig. 3*C*), PKCβII was found also to translocate to intracellular structures in response to KCl. The identity of the majority of these structures was revealed as mature insulin secretory vesicles by simultaneous imaging of a co-expressed dense core vesicle membrane protein, phogrin (39), conjugated to cyan fluorescent protein (47).

Changes in $[Ca^{2+}]_c$ in the bulk cytosol and beneath the membrane in response to cell depolarization induced by KCl or tolbutamide were explored with targeted pericams. In contrast to untargeted pericam, which reported an increase in intracel-

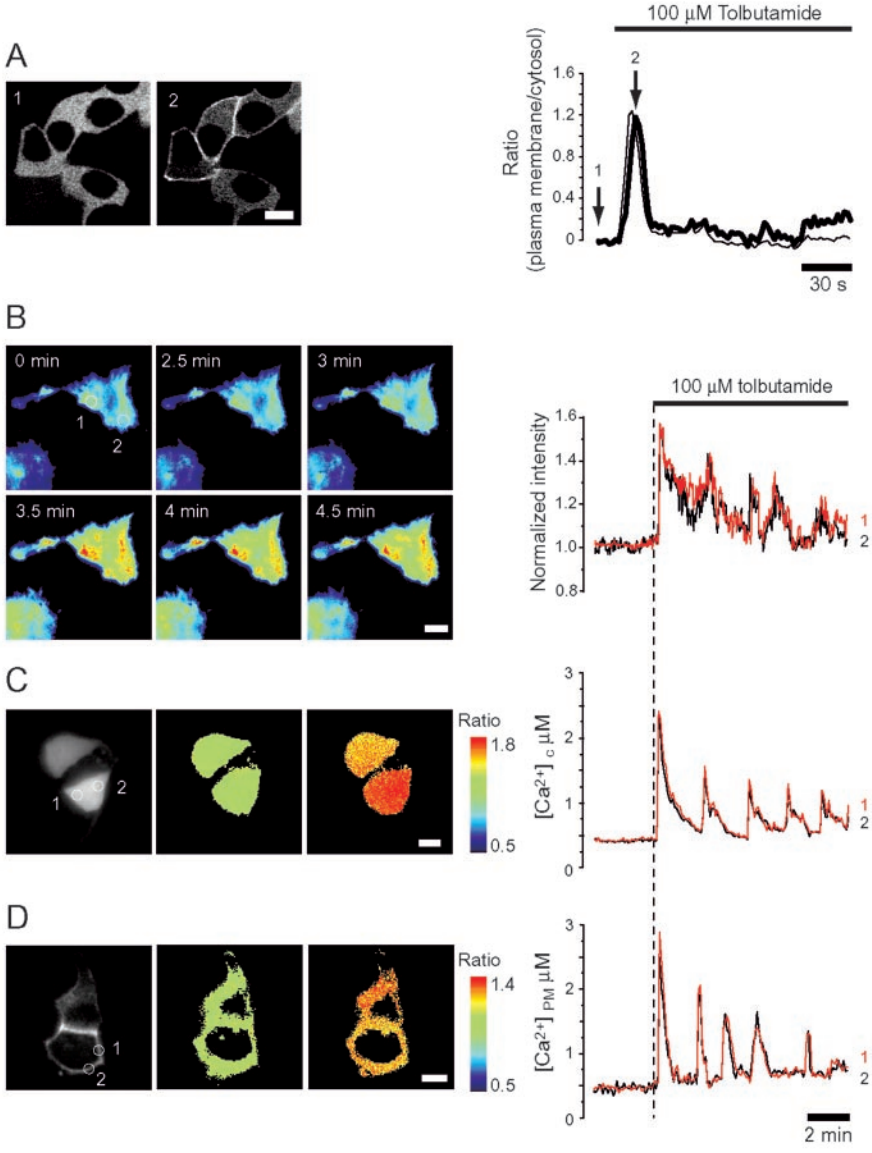

FIG. 4. **Effect of K_{ATP} channel closure on PKC·βII distribution (*A*, *B*) and intracellular Ca^{2+} changes (*C*, *D*).** Cells expressing either PKCβII (*A*, *B*), or targeted pericams were incubated with the indicated concentrations of tolbutamide. Other details as Fig. 2.

lular Ca^{2+} upon cell depolarization to 1.38 ± 0.26 μM (n = 20 cells; Fig. 3*D*), plasma membrane localized SNAP25·pericam reported an increase to 1.82 ± 0.31 μM (n = 20 cells, $p < 0.05$ with respect to cytosolically targeted pericam; Fig. 3*E*).

Simultaneous Imaging of PKCβII Translocation and Depolorization-induced $[Ca^{2+}]_c$ Increases in Single Cells—We next sought evidence that the larger increase in Ca^{2+} beneath the plasma membrane may be important for the recruitment of PKCβII·EGFP. If the glucose-induced translocation of PKCβII were due solely to a global increase in intracellular $[Ca^{2+}]_c$, it would be predicted that the kinetics of the increases in $[Ca^{2+}]_c$ and the membrane content of PKCβII would be very similar. Indeed, glucose induced changes in PKCβII·EGFP distribution, and cytosolic Ca^{2+} displayed grossly similar kinetics (Fig. 2, *A* and *B versus C* and *D*). However, when cells were stimulated with KCl, this prediction only held true during the initial recruitment of the chimera (see Fig. 6). At later time points (>30 s) PKCβII·EGFP dissociated from the membrane while $[Ca^{2+}]_c$ remained close to maximal. These data suggest that PKCβII association with the plasma membrane may be controlled by locally high Ca^{2+} concentrations.

Impact of Intracellular Ca^{2+} Mobilization on PKCβII Localization—Activation of muscarinic receptors with carbachol and mobilization of intracellular Ca^{2+} caused a rapid, transient translocation to the plasma membrane (in 25 of 29 cells examined, Fig. 5, *A* and *B*). This effect was entirely blocked by the presence of the phospholipase C inhibitor U73122 (Fig. 5*B*, *trace 3*). In contrast to depolarizing stimuli (Figs. 3 and 4) carbachol caused an essentially identical increase in $[Ca^{2+}]_{PM}$ (to 2.62 ± 0.42 μM, n = 10 cells; Fig. 5*D*) as $[Ca^{2+}]_c$ (to 2.48 ± 0.36 μM, n = 10 cells; Fig. 5*C*). Interestingly, the response to carbachol was significantly accelerated at high glucose concentrations (Fig. 5*A*, *images 3* and *4* and *lower graph*; *solid versus dashed trace*), presumably reflecting glucose-induced Ca^{2+} influx and/or DAG production (see "Discussion").

Effects of Glucose on the Subcellular Distribution of Novel and Atypical PKC Isoforms—The ineffectiveness of the phospholipase C inhibitor to prevent glucose or KCl-induced recruitment of PKCβII to the plasma membrane (Fig. 3*B*) suggested that DAG production and binding to C1 domains may have played a relatively small part in translocation. In line with this view, the distribution of neither the novel isoform PKCδ (no C2 domain) (48) nor PKCζ (lacking both C1 and C2 domains) were affected by glucose (Fig. 7) or depolarizing stimuli (not shown). By contrast, PKCδ was rapidly translocated (half-time ~20 s in each case) to both the nuclear membrane and cell surface in response to addition of the phorbol ester, PMA (Fig. 7, *A* and *B*).

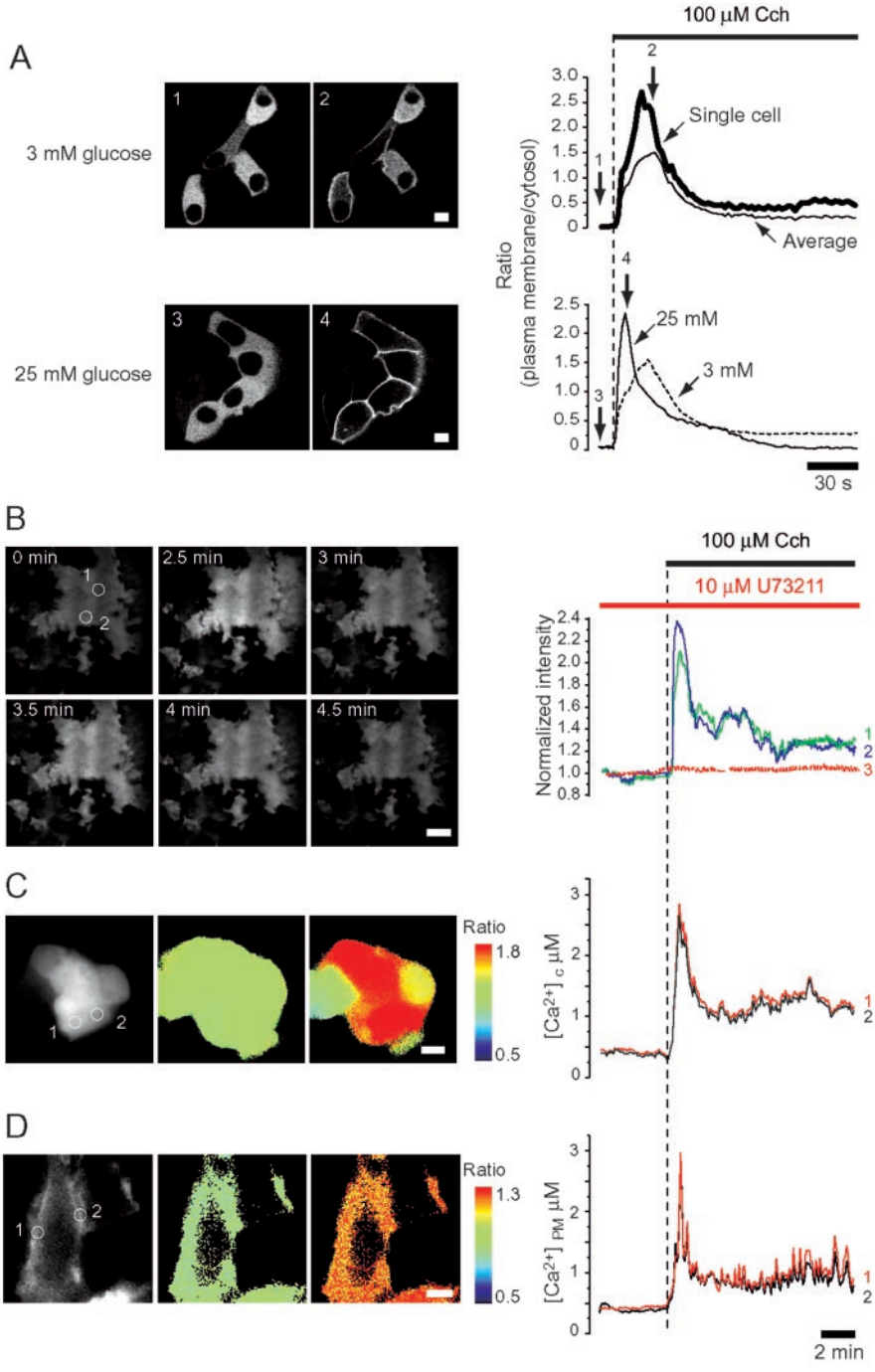

FIG. 5. **Effect of carbachol on PKC·βII distribution (*A*, *B*) and intracellular [Ca^{2+}] changes (*C*, *D*).** Cells expressing either PKCβII (*A*, *B*) or targeted pericams were incubated with the indicated concentrations of carbachol (*Cch*). The upper trace in *A* shows the response of the represented cell (1, 2; *black trace*) or the average of eight other cells (*gray trace*). The lower images (3, 4) and time course show the effect of preincubation for 300 s at 25 mM glucose (*solid trace* in the graph; mean of six cells). Shown for comparison are the kinetics of redistribution observed at 3 mM glucose (*dashed trace*). The average peak ratios were 2.29 ± 0.57 at 25 mM glucose and 1.58 ± 0.38 at 3 mM glucose. Corresponding time-to-peaks were 8.2 ± 0.92 s and 19.1 ± 2.6 s ($p < 0.05$ for the effect of 25 *versus* 3 mM glucose). Other details are as Fig. 2.

DISCUSSION

Dynamics of PKCβII·EGFP Translocation—We show here, for the first time in single living β-cells, that elevated glucose concentrations cause complex and dynamic changes in the localization of a conventional PKC isoform PKCβII. This behavior was observed in both primary islet β-cells (Fig. 1*A*) and, more dramatically, in clonal MIN6 β-cells (Fig. 2, *A* and *B*). In the latter case, TIRF microscopy revealed the creation by elevated glucose concentrations of hot spots and waves of PKCβII at the plasma membrane (see also movie "Fig. 2*B*" at *http://www.jbc.org*). In this respect, the behavior of PKCβII (9) as well as the conventional PKC isoforms PKCγ (6) and PKCα (7) is reminiscent of that previously described in non-excitable cells using GFP chimeras and confocal microscopy. However, by the use of TIRF microscopy, we also reveal the creation by elevated glucose concentrations of hot spots and waves of PKCβII at the plasma membrane, phenomena recently described for PKCλ in astrocytes (49). Arguing against the possibility that this behavior reflects a nonspecific coagulation of GFP molecules on the membrane, such hot spots are rarely observed using phospholipid-dependent membrane-targeted EGFP chimeras that incorporate pleckstrin homology domains using either confocal (50) or TIRF microscopy.[2] The present data are also consistent with the findings of Yedovitzky *et al*. (4) and Ganesan *et al*. (3) who demonstrated the translocation of PKCα to the plasma membrane of β-cells by immunocytochemistry and biochemical analyses, respectively.

[2] T. Tsuboi, Q. Qian, and G. A. Rutter, unpublished observations.

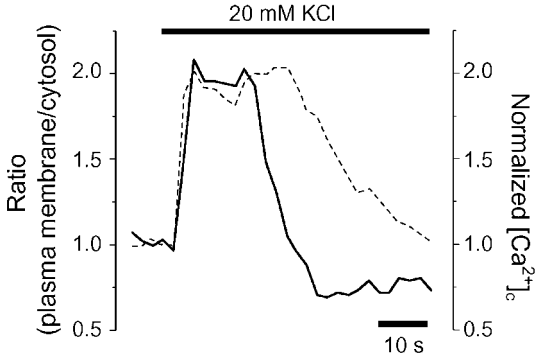

FIG. 6. **Cytosolic relocation of PKCβII precedes the decay in $[Ca^{2+}]$ following K^+-induced membrane depolarization.** The time course of $[Ca^{2+}]_c$ elevation following stimulation with 20 mM KCl was monitored using Calcium Crimson in a single cell infected with virus PKCβII·EGFP. Elevation of $[Ca^{2+}]_c$ was reported as a relative increase in Calcium Crimson fluorescence compared with unstimulated conditions. Plasma membrane localization of PKCβII·EGFP was recorded as a relative increase in the ratio of EGFP fluorescence in the vicinity of the plasma membrane to that of the bulk cytosol. Images were acquired every 2 s. The trace is a single cell representative of five cells from three separate experiments.

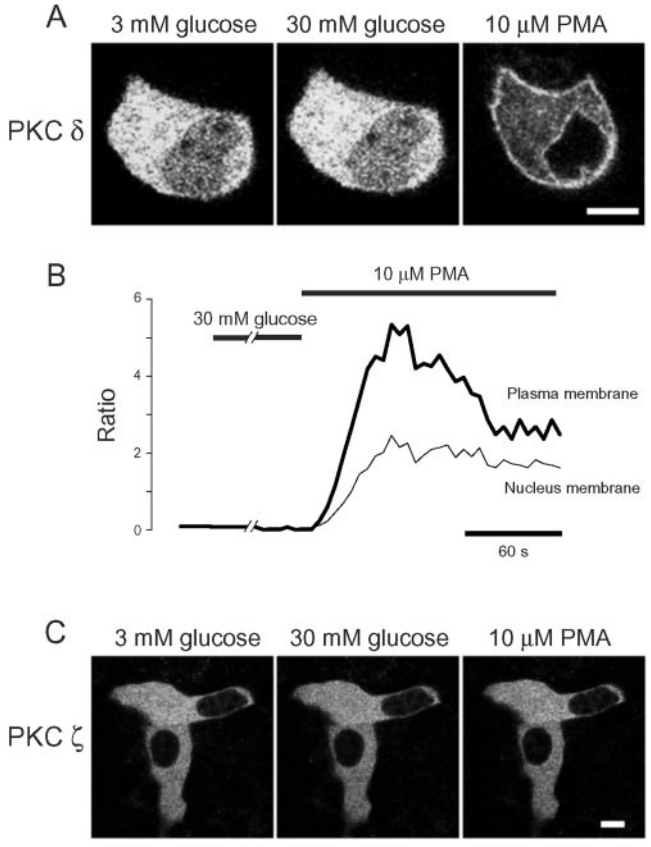

FIG. 7. **Effects of glucose and PMA on the subcellular distribution of PKCδ-EGFP (*A*, *B*) and PKCζ-EGFP (*C*) in MIN6 cells.** *A*, cells expressing PKCδ-EGFP were incubated in KRB containing 3 mM glucose and stimulated with 25 mM glucose for 300 s, prior to addition of 10 μM PMA. Images were collected using the confocal microscope at the start of the incubation, 300 s after the addition of 25 mM glucose, and 300 s after the subsequent addition of PMA. *B*, time course of changes in fluorescence at the plasma membrane and nuclear membrane in the single cell shown in *A*. *C*, cells expressing PKCζ-EGFP were imaged during identical manipulations to those described in *A*.

Interestingly, we failed to find any change in the localization of either PKCδ or PKCζ in response to glucose or other secretagogue stimuli (Fig. 7). These results contrast with reports of an important role of PKCζ in the regulation of the preproinsulin gene by glucose (51), although it should be emphasized that we did not explore the localization of this isoform beyond relatively short (~30 min) time points after glucose stimulation.

Mechanisms Involved in PKCβII Translocation, Role of Ca^{2+} Microdomains—We provide evidence that the changes in PKCβII distribution are likely to result from localized changes in cytosolic Ca^{2+} concentration generated beneath the plasma membrane during the depolarization-induced opening of L-type Ca^{2+} changes (15). Thus, depolarizing concentrations of KCl (Fig. 3, *D* and *E*) or tolbutamide (Fig. 4, *C* and *D*) increased $[Ca^{2+}]_c$ in this domain ($[Ca^{2+}]_{PM}$) to concentrations 1.3–1.5-fold higher than those in the bulk cytosol and caused robust translocation of PKCβII·EGFP to the membrane. However, the partial inhibition of glucose-induced PKCβII translocation by blockade of phospholipase C activity (Fig. 2*B*, *trace 5*) suggests that the local generation of DAG, caused by phospholipid hydrolysis, may contribute to the recruitment of conventional PKCs to the membrane in response to glucose. In this regard it should be mentioned that total islet DAG content is reported to increase only slightly (52) if at all (53) at elevated glucose concentrations, largely through *de novo* synthesis of DAG from glucose-derived palmitate (52). Importantly, such changes are not expected to be blocked by inhibitors of phospholipase C (Fig. 2*B*). However, arguing that glucose-induced increases in DAG content are small in the MIN6 cell system studied here, we failed to observed any translocation of PKCδ to the cell surface in response to elevated glucose concentrations (Fig. 7, *A* and *B*). On the other hand, because PKCα activity is regulated by several long chain acyl-CoA esters (54), a possible role for glucose-induced increase in the concentrations of these latter species (55) in the observed recruitment of PKCβII to the plasma membrane cannot be ruled out.

Our observations (Fig. 6) that cytosolic $[Ca^{2+}]$ and PKC membrane localization could be dissociated in the same single cell are perhaps most simply explained by the fact that in the absence of generation of DAG a "threshold" concentration of Ca^{2+}, probably ≥ 1 μM, is required to ensure the binding of the C2 domain of PKCβII to membrane phospholipids (44) as previously proposed for PKCα (56). Interestingly, the concentrations of Ca^{2+} measured here immediately beneath the membrane of stimulated MIN6 β-cells (2–3 μM) are similar to, if somewhat lower than, those previously reported at greater distances from the plasma membrane (0.5–1.0 μm) of β-cells using diffusible dyes (6–10 μM) (57). Thus, the present data, which were obtained using a molecularly targeted probe, would seem to rule out the notion of a generalized large gradient of Ca^{2+} concentration stretching across the whole interior surface of the cell membrane. However, more localized $[Ca^{2+}]_c$ domains (for example at the mouth of individual Ca^{2+} channels) (58, 59) cannot be excluded. In contrast to the impact of stimulated Ca^{2+} influx, the stimulation of intracellular Ca^{2+} release and DAG production with a muscarinic agonist elicited efficient membrane localization of PKCβII (Fig. 5), presumably reflecting a slightly larger increase in plasma membrane $[Ca^{2+}]_c$ as well as the cooperation of C1 and C2 domains in membrane association (44). Interestingly, this effect of carbachol was significantly accelerated by elevated glucose concentrations (see legend to Fig. 5), possibly reflecting the *de novo* synthesis of DAG from glucose (52).

Potential Roles of PKCβII Translocation in Regulated Insulin Secretion and Gene Expression—What may be the consequences of the translocation of PKCβII (and other conventional PKCs) to the plasma membrane? Arguing that the enzyme is at least partly activated upon membrane translocation in β-cells, only kinase-active PKCβII, but not an active site (K371R) mu-

tant, was found to retranslocate into the cytosol after antigen stimulation of HEK 293 cells (9). Although targets of PKC are not well characterized in the β-cell, possibilities include both the pore-forming subunit of K_{ATP} channels (60) and proteins of the secretory machinery (*e.g.* SNAP25) (61, 62).

By demonstrating that activated PKCβII can migrate to the surface of secretory vesicles (Fig. 3*C*) the current studies provide evidence for a new mechanism whereby vesicle fusion may be controlled locally. Thus, efflux of stored Ca^{2+} from vesicles (40, 63), possibly by gating of vesicle-associated receptors for ryanodine (63) or nicotinic acid adenine dinucleotide phosphate (64),[3] may lead to the recruitment of the kinase to a highly localized domain of $[Ca^{2+}]$ at the vesicle surface. A similar mechanism has recently been proposed for the translocation of PKCα to internal ryanodine receptor-gated Ca^{2+} release sites in vascular smooth muscle cells (65).

Acknowledgments— We thank the Bristol Medical Research Council Cell Imaging Facility for assistance with single cell imaging and The Wellcome Trust/Higher Education Funding Council for a Joint Infrastructure Award. We are indebted to Dr. A. Miyawaki (RIKEN, Saitama, Japan) for the kind gifts of pericam expression constructs.

REFERENCES

1. Nishizuka, Y. (1988) *Nature* **334,** 661–665
2. Deeney, J. T., Cunningham, B. A., Chheda, S., Bokvist, K., Juntti-Berggren, L., Lam, K., Korchak, H. M., Corkey, B. E., and Berggren, P. O. (1996) *J. Biol. Chem.* **271,** 18154–18160
3. Ganesan, S., Calle, R., Zawalich, K., Smallwood, J. I., Zawalich, W. S., and Rasmussen, H. (1990) *Proc. Natl. Acad. Sci. U. S. A.* **87,** 9893–9897
4. Yedovitzky, M., MochlyRosen, D., Johnson, J. A., Gray, M. O., Ron, D., Abramovitch, E., Cerasi, E., and Nesher, R. (1997) *J. Biol. Chem.* **272,** 1417–1420
5. Tsien, R. Y. (1998) *Annu. Rev. Biochem.* **67,** 509–544
6. Sakai, N., Sasaki, K., Ikegaki, N., Shirai, Y., Ono, Y., and Saito, N. (1997) *J. Cell Biol.* **139,** 1465–1476
7. Oancea, E., and Meyer, T. (1998) *Cell* **95,** 307–318
8. Chiesa, A., Rapizzi, E., Tosello, V., Pinton, P., de Virgilio, M., Fogarty, K. E., and Rizzuto, R. (2001) *Biochem. J.* **355,** 1–12
9. Feng, X., and Hannun, Y. A. (1998) *J. Biol. Chem.* **273,** 26870–26874
10. Graham, M. E., Fisher, R. J., and Burgoyne, R. D. (2000) *Biochimie* (*Paris*) **82,** 469–479
11. Rutter, G. A. (2001) *Mol. Aspects Med.* **22,** 247–284
12. Matschinsky, F. M., Ghosh, A. K., Meglasson, M. D., Prentki, M., June, V., and Von Allman, D. (1986) *Biol. Chem.* **261,** 14057–14061
13. Kennedy, H. J., Pouli, A. E., Jouaville, L. S., Rizzuto, R., and Rutter, G. A. (1999) *J. Biol. Chem.* **274,** 13281–13291
14. Bryan, J., and AguilarBryan, L. (1997) *Curr. Opin. Cell Biol.* **9,** 553–559
15. Safayhi, H., Haase, H., Kramer, U., Bihlmayer, A., Roenfeldt, M., Ammon, H. P., Froschmayr, M., Cassidy, T. N., Morano, I., Ahlijanian, M. K., and Striessnig, J. (1997) *Mol. Endocrinol.* **11,** 619–629
16. Lang, J. C. (1999) *Eur. J. Biochem.* **259,** 3–17
17. Tanigawa, K., Kuzuya, H., Imura, H., Taniguchi, H., Baba, S., Takai, Y., and Nishizuka, Y. (1982) *FEBS Lett.* **138,** 183–186
18. Lord, J. M., and Ashcroft, S. J. (1984) *Biochem. J.* **219,** 547–551
19. Zawalich, W., Brown, C., and Rasmussen, H. (1983) *Biochem. Biophys. Res. Commun.* **117,** 448–455
20. Tian, Y. M., Urquidi, V., and Ashcroft, S. J. H. (1996) *Mol. Cell. Endocrin.* **119,** 185–193
21. Onoda, K., Hagiwara, M., Hachiya, T., Usuda, N., Nagata, T., and Hidaka, H. (1990) *Endocrinology* **126,** 1235–1240
22. Arkhammar, P., Juntti-Berggren, L., Larsson, O., Welsh, M., Nanberg, E., Sjoholm, A., Kohler, M., and Berggren, P. O. (1994) *J. Biol. Chem.* **269,** 2743–2749
23. Kaneto, H., Suzuma, K., Sharma, A., Bonner-Weir, S., King, G. L., and Weir, G. C. (2002) *J. Biol. Chem.* **277,** 3680–3685
24. Easom, R. A., Hughes, J. H., Landt, M., Wolf, B. A., Turk, J., and McDaniel, M. L. (1989) *Biochem. J.* **264,** 27–33
25. Bozem, M., Nenquin, M., and Henquin, J. C. (1987) *Endocrinology* **121,** 1025–1033
26. Ammala, C., Eliasson, L., Bokvist, K., Berggren, P. O., Honkanen, R. E., Sjoholm, A., and Rorsman, P. (1994) *Proc. Natl. Acad. Sci. U. S. A.* **91,** 4343–4347
27. Zawalich, W. S., and Rasmussen, H. (1990) *Mol. Cell. Endocrinol.* **70,** 119–137
28. Zawalich, W. S., and Zawalich, K. C. (2001) *Mol. Cell. Endocrinol.* **177,** 95–105
29. Arkhammar, P., Nilsson, T., Welsh, M., Welsh, N., and Berggren, P. O. (1989) *Biochem. J.* **264,** 207–215
30. Axelrod, D. (1981) *J. Cell Biol.* **89,** 141–145
31. Toomre, D., and Manstein, D. J. (2001) *Trends Cell Biol.* **11,** 298–303
32. Tsuboi, T., Zhao, C., Terakawa, S., and Rutter, G. A. (2000) *Curr. Biol.* **10,** 1307–1310
33. Tsuboi, T., Kikuta, T., Warashina, A., and Terakawa, S. (2001) *Biochem. Biophys. Res. Commun.* **282,** 621–628
34. Tsuboi, T., Terakawa, S., Scalettar, B. A., Fantus, C., Roder, J., and Jeromin, A. (2002) *J. Biol. Chem.* **277,** 15957–15961
35. Nagai, T., Sawano, A., Park, E. S., and Miyawaki, A. (2001) *Proc Nat. Acad Sci U. S. A.* **98,** 3197–3202
36. He, T. C., Zhou, S., da Costa, L. T., Yu, J., Kinzler, K. W., and Vogelstein, B. (1998) *Proc. Natl. Acad. Sci. U. S. A.* **95,** 2509–2514
37. Ainscow, E. K., Zhao, C., and Rutter, G. A. (2000) *Diabetes* **49,** 1149–1155
38. Ainscow, E. K., and Rutter, G. A. (2001) *Biochem. J.* **353,** 175–180
39. Wasmeier, C., and Hutton, J. C. (1996) *J. Biol. Chem.* **271,** 18161–18170
40. Pouli, A. E., Emmanouilidou, E., Zhao, C., Wasmeier, C., Hutton, J. C., and Rutter, G. A. (1998) *Biochem. J.* **333,** 193–199
41. Emmanouilidou, E., Teschemacher, A., Pouli, A. E., Nicholls, L. I., Seward, E. P., and Rutter, G. A. (1999) *Curr. Biol.* **9,** 918
42. Grynkiewicz, G., Poenie, M., and Tsien, R. Y. (1985) *J. Biol. Chem.* **260,** 3440–3450
43. Miyazaki, J., Araki, K., Yamato, E., Ikegami, H., Asano, T., Shibasaki, Y., Oka, Y., and Yamamura, K. (1990) *Endocrinology* **127,** 126–132
44. Sanderson, M. J. (1995) *CIBA Found. Symp.* **188,** 175–189
45. Nalefski, E. A., and Newton, A. C. (2001) *Biochemistry* **40,** 13216–13229
46. Nalefski, E. A., Slazas, M. M., and Falke, J. J. (1997) *Biochemistry* **36,** 12011–12018
47. Sudhof, T. C. (1995) *Nature* **375,** 645–653
48. Zhang, G., Kazanietz, M. G., Blumberg, P. M., and Hurley, J. H. (1995) *Cell* **81,** 917–924
49. Codazzi, F., Teruel, M. N., and Meyer, T. (2001) *Curr. Biol.* **11,** 1089–1097
50. Venkateswarlu, K., Oatey, P. B., Tavare, J. M., and Cullen, P. J. (1998) *Curr. Biol.* **8,** 463–466
51. Furukawa, N., Shirotani, T., Araki, E., Kaneko, K., Todaka, M., Matsumoto, K., Tsuruzoe, K., Motoshima, H., Yoshizato, K., Kishikawa, H., and Shichiri, M. (1999) *Endocr. J.* **46,** 43–58
52. Peter-Riesch, B., Fathi, M., Schlegel, W., and Wollheim, C. B. (1988) *J. Clin. Invest.* **81,** 1154–1161
53. Wolf, B. A., Easom, R. A., McDaniel, M. L., and Turk, J. (1990) *J. Clin. Invest.* **85,** 482–490
54. Yaney, G. C., Korchak, H. M., and Corkey, B. E. (2000) *Endocrinology* **141,** 1989–1998
55. Corkey, B. E., Deeney, J. T., Yaney, G. C., Tornheim, K., and Prentki, M. (2000) *J. Nutr.* **130,** 299S–304S
56. Khalil, R. A., Lajoie, C., and Morgan, K. G. (1994) *Am. J. Physiol.* **266,** C1544–C1551
57. Quesada, I., Martin, F., and Soria, B. (2000) *J. Physiol.* **525,** 159–167
58. Neher, E., and Augustine, G. J. (1992) *J. Physiol.* **450,** 273–301
59. Wiser, O., Trus, M., Hernandez, A., Renstrom, E., Barg, S., Rorsman, P., and Atlas, D. (1999) *Proc. Natl. Acad. Sci. U. S. A.* **96,** 248–253
60. Light, P. E., Bladen, C., Winkfein, R. J., Walsh, M. P., and French, R. J. (2000) *Proc. Natl. Acad. Sci. U. S. A.* **97,** 9058–9063
61. Shimazaki, Y., Nishiki, T., Omori, A., Sekiguchi, M., Kamata, Y., Kozaki, S., and Takahashi, M. (1996) *J. Biol. Chem.* **271,** 14548–14553
62. Genoud, S., Pralong, W., Riederer, B. M., Eder, L., Catsicas, S., and Muller, D. (1999) *J. Neurochem.* **72,** 1699–1706
63. Mitchell, K., Pinton, P., Varadi, A., Ainscow, E. K., Pozzan, T., Rizzuto, R., and Rutter, G. A. (2001) *J. Cell Biol.* **155,** 41–51
64. Patel, S., Churchill, G. C., and Galione, A. (2001) *Trends Biochem. Sci.* **26,** 482–489
65. Maasch, C., Wagner, S., Lindschau, C., Alexander, G., Buchner, K., Gollasch, M., Luft, F. C., and Haller, H. (2000) *FASEB J.* **14,** 1653–1663

[3] K. J. Mitchell and G. A. Rutter, unpublished data.